

Two-dimensional nonlocal model of axially and radially inhomogeneous plasma of cylindrical magnetron discharge

I. A. Porokhova,^{1,2} Yu. B. Golubovskii,² M. Holík,^{1,3} P. Kudrna,^{1,3} M. Tichý,^{1,3} C. Wilke,¹ and J. F. Behnke¹

¹*Institute for Physics, Ernst-Moritz-Arndt University, Domstrasse 10a, D-17487 Greifswald, Germany*

²*St. Petersburg State University, Ulianovskaia 1, 195904 St. Petersburg, Russia*

³*Charles University in Prague, V Holešovičkách 2, 18000 Prague, Czech Republic*

(Received 8 October 2002; published 3 July 2003)

A cylindrical magnetron discharge (CMD) with two coaxial electrodes, a uniform axially directed magnetic field, and discharge ends closed by the shields biased at the cathode potential is considered. The presence of the shields creates axial inhomogeneity of plasma, which is taken into account in this study. At low pressures and small magnetic fields the pronounced nonlocal regime of the electron distribution function (EDF) formation is realized. The electron component is analyzed on the basis of radially and axially inhomogeneous Boltzmann kinetic equation. Unmagnetized electrons that move in axial direction are trapped in the axial potential well, their energy relaxation length exceeds the discharge vessel length, and the kinetic equation can be averaged over axial flights of electrons. Using a model two-dimensional potential profile, the EDFs at the different axial positions are obtained and two-dimensional distributions of the electron density, ionization rate, and current on cathode are calculated. The results of the modeling and experiments are compared for the dc CMD in Ar at a pressure of 3 Pa, magnetic field strength of 10 mT, and current of 150 mA.

DOI: 10.1103/PhysRevE.68.016401

PACS number(s): 52.25.Xz, 52.25.Dg

I. INTRODUCTION

Magnetron glow discharges are widely used in the thin-film processing industry and coating applications. Magnetron devices differ from conventional glow discharges by employing externally applied magnetic field, which is parallel to the cathode surface in a certain region, as it is in the planar or geometrically complicated discharges, or in a whole region, as it is in the cylindrical magnetrons. A transverse field configuration leads to the electron confinement and increase in plasma density, thus yielding higher ion production and higher sputtering rates [1].

A big variety of the electric and magnetic field configurations has been used in the magnetron sputtering discharges. Most commonly, experimental and theoretical researches focus on the planar magnetrons [2–4] and cylindrical magnetrons [5–8].

Numerous discharge models have been developed to determine plasma parameters such as the charged particle densities and temperatures, the plasma potential, and the electron distribution functions (EDF) [4,5,9,10]; other studies consider various physical processes occurring on the film surface and in its vicinity [11,12]. Most often two classes of computational techniques are used for the modelings, these are PIC-MCC methods and fluid one-dimensional analysis. The fluid methods describe magnetron plasma in terms of the Townsend ionization coefficient and classical transport that assumes Maxwell distribution and local mechanism of the EDF formation. The magnetron discharges operate at very low pressures yielding nonequilibrium nonlocal distribution functions. Therefore, strictly saying, the fluid approaches are unapplicable to magnetron plasma. PIC simulations being fully kinetic and self-consistent are a powerful tool for the treatment of the nonequilibrium distribution functions, although there are several drawbacks caused by their compu-

tational expenses and sensitivity to numerical noise. In addition, a majority of papers reveals either no comparison with experimental results or poor agreement between calculations and measurements, which hampers estimating the efficiency of the models.

In this paper the cylindrical magnetron discharge (CMD) is considered, which due to its relatively simple geometry and field configuration is an interesting topic for the experimental studies and modelings. In the series of our works the CMD has been extensively studied experimentally [13–16] by Langmuir probe to detect an electron behavior and by laser absorption technique to detect metastable and resonance atom distributions, as well as by the one-dimensional (1D) nonlocal kinetic [8,17] and PIC [18] modelings. Although the comparison of the measured and calculated results revealed a satisfactory agreement in the most of investigated plasma parameters, namely, the plasma density, electron average energy, high-energy parts of the EDFs, and densities of excited states [17], there was some discrepancy between experiment and theories, which was supposed to be caused by the axial inhomogeneity and edge effects not included in the models. Recent experimental investigations performed in the novel CMD [19], which is three times longer than the previous one and contains a segmented cathode, showed that there is significant steady-state axial variation of the plasma parameters, which becomes more pronounced at higher pressures and larger magnetic fields. At small magnetic fields ($B < 20$ mT) the axial distributions of the plasma parameters were flat with the exception of the periphery regions disturbed by the shields.

In the present paper we develop a two-dimensional nonlocal kinetic model of the cylindrical magnetron discharge, which apart from the radial structure caused by the current flow takes into account the plasma axial inhomogeneity created by the shields at the ends. So far, these edge effects remained outside the frames of the fluid models, as well as

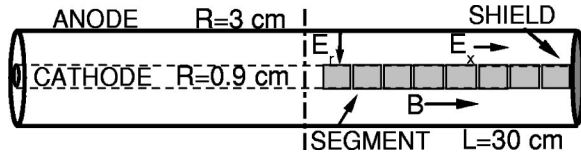


FIG. 1. Schematic view of the CMD. The cathode and anode are the coaxial cylinders. The uniform magnetic field is directed axially. Shields are connected to the cathode. The left shield is not shown for clarity.

PIC simulations. The electron kinetics in inhomogeneous axial and radial fields will be considered based on numerical solving the kinetic Boltzmann equation. The nonlocal approach will be applied, and the distribution functions of the electrons will be calculated. Calculations of axial and radial variations of plasma density, ionization rate, and current densities will yield an explanation of the axial inhomogeneities observed in the experiment. Particular results of experiment and modeling refer to dc discharge in Ar at a pressure of 3 Pa, magnetic field strength of 10 mT, and current of 150 mA.

II. A DESCRIPTION OF THE CMD

The cylindrical magnetron discharge used in this study is a modification of the original design described in detail in Ref. [16]. The cylindrical discharge vessel that serves as an anode (grounded) is 30 cm in length and 5.8 cm in diameter. The diameter of the inner coaxial cathode is 1.8 cm. The ratio of length to radius hence equals 15. Such a large value of the length-to-radius ratio was designed to provide axial homogeneity of the discharge in the center region and to provide possibility of using the one-dimensional computational models. Six evenly distributed coils create the axially homogeneous magnetic field. The system is equipped with three cylindrical Langmuir probes movable in radial direction, placed in ports located between each couple of coils at a distance of 6 cm from each other. Half of the cathode length is segmented into seven segments of length 2.0 cm each. The segments are distanced from each other by 1 mm and isolated by teflon material. The other half of the cathode is not segmented. Both the segmented and nonsegmented parts of the cathode are water cooled. Two ends of the device are closed with stainless steel disks (shields) that are connected to the cathode, and hence biased at the cathode potential V_c . The schematic view of the cylindrical magnetron discharge is shown in Fig. 1.

The limiters (shields), being at high negative potential, influence plasma by creating extended sheaths, which disturb axial homogeneity. Using three Langmuir probes located along the discharge length, the radial profiles of the electron density can be measured simultaneously for these axial points. The segmented cathode enables the measurement of the axial variations of the discharge current. The measurements of the discharge voltage, electron density, and distribution of current on cathode [19] are the basis for development of the two-dimensional models.

III. THE BASIC EQUATIONS

An electron behavior in the axially and radially inhomogeneous CMD will be analyzed based on the spatially inhomogeneous Boltzmann equation,

$$\vec{v} \cdot \nabla_{\vec{r}} F - \frac{e}{m} (\vec{E} + [\vec{v} \times \vec{B}]) \cdot \nabla_{\vec{v}} F = C(F), \quad (1)$$

where m and $-e$ are the mass and charge of the electron. The electron distribution function (EDF) $F(\vec{v}, \vec{r})$ is formed under the influence of the spatial gradients, actions of the axial magnetic field \vec{B} , electric field \vec{E} which has radial and axial components, and the collision processes $C(F)$. Employing a two-term expansion of the EDF in spherical harmonics, the electron distribution can be represented in the form

$$F(\vec{v}, \vec{r}) = F_0(v, r, x) + \vec{F}_1(v, r, x) \cdot \frac{\vec{v}}{v} = F_0(v, r, x) + \frac{v_r}{v} F_{1r}(v, r, x) + \frac{v_\theta}{v} F_{1\theta}(v, r, x) + \frac{v_x}{v} F_{1x}(v, r, x), \quad (2)$$

where F_0 is the isotropic distribution and F_{1r} , $F_{1\theta}$, and F_{1x} are the radial, azimuth, and axial components of the vector EDF anisotropy. A range of applicability of the two-term expansion has been discussed in Ref. [8]. Taking into account the higher terms of the expansion will incredibly complicate the problem, while an error in macroscopic properties is expected to be less than 10% according to the multiterm study [20].

Substitution of expansion (2) into the kinetic equation (1), and integration over solid angles yields

$$\frac{v}{3} \nabla_{\vec{r}} \cdot \vec{F}_1 - \frac{e}{3m} \frac{1}{v^2} \frac{\partial}{\partial v} (v^2 \vec{E} \cdot \vec{F}_1) = C_0,$$

$$v \nabla_{\vec{r}} F_0 - \frac{e \vec{E}}{m} \frac{\partial F_0}{\partial v} - \frac{e}{m} [\vec{B} \times \vec{F}_1] = \vec{C}_1.$$

Taking into account that $\vec{E} = E_r \vec{e}_r + E_x \vec{e}_x$, $\vec{B} = B \vec{e}_x$, and $\vec{C}_1 = -(v/\lambda_e) \vec{F}_1$ (λ_e is electron free path), we obtain the following expressions for the anisotropic components:

$$f_{1r}(U, r, x) = \frac{\lambda_e}{1 + (\lambda_e/r_{ec})^2} \left[-\frac{\partial f_0}{\partial r} + e E_r \frac{\partial f_0}{\partial U} \right], \quad (3)$$

$$f_{1x}(U, r, x) = \lambda_e \left[-\frac{\partial f_0}{\partial x} + e E_x \frac{\partial f_0}{\partial U} \right], \quad (4)$$

$$f_{1\theta}(U, r, x) = \frac{\lambda_e}{r_{ec}} f_{1r}(U, r, x),$$

where $r_{ec} = v/\omega_{eB}$ is the radius of electron cyclotron motion, $\omega_{eB} = eB/m$ is the cyclotron frequency, and $U = mv^2/2$ is the kinetic energy. The functions F and f differ by the normalization factor $2\pi(2/m)^{3/2}$.

It is seen from Eqs. (3) and (4) that the magnetic field does not influence the axial anisotropy, whereas it reduces the radial anisotropic distribution by the factor $(r_{ec}/\lambda_e)^2$. Thus, the axial transport of the electrons remains unaffected by the magnetic field, and this in the radial direction is stipulated by the $E \times B$ drift.

The kinetic equation for the isotropic distribution function is

$$\begin{aligned} & \frac{U}{3} \frac{1}{r} \frac{\partial}{\partial r} r f_{1r} - \frac{eE_r}{3} \frac{\partial}{\partial U} U f_{1r} + \frac{U}{3} \frac{\partial}{\partial x} f_{1x} - \frac{eE_x}{3} \frac{\partial}{\partial U} U f_{1x} \\ & = S_0(f_0), \end{aligned} \quad (5)$$

where the collision operator

$$S_0(f_0) = S_0^{el}(f_0) + S_0^{ex}(f_0) + S_0^{ion}(f_0)$$

includes elastic, inelastic, and ionization collisions,

$$S_0^{el}(f_0) = 2 \frac{m}{M} \frac{\partial}{\partial U} [U^2 N Q_{el}(U) f_0(U, r)],$$

$$\begin{aligned} S_0^{ex}(f_0) &= -UNQ_{ex}(U) f_0(U, r) + (U + U_{ex})N \\ & \times Q_{ex}(U + U_{ex}) f_0(U + U_{ex}, r), \end{aligned}$$

$$\begin{aligned} S_0^{ion}(f_0) &= \sum \{ -UN_A Q_i(U) f_0(U, r) + (U/\beta + U_i) \\ & \times N_A Q_i(U/\beta + U_i) f_0(U/\beta + U_i, r)/\beta \\ & + (U/(1-\beta) + U_i) N_A Q_i(U/(1-\beta) + U_i) \\ & \times f_0(U/(1-\beta) + U_i, r)/(1-\beta) \}. \end{aligned}$$

Here $Q_{el}(U)$ and $Q_{ex}(U)$ are the transport cross sections for momentum transfer and excitation with the threshold U_{ex} . M is the atom mass, and β and $(1-\beta)$ are the fractions in which the remaining energy of the colliding electron is shared in ionization event between the two outgoing electrons. The ionization operator S_0^{ion} includes a sum of direct and stepwise ionization, where the ionization cross section Q_i denotes either that of direct ionization (Q_{di}) or stepwise ionization (Q_{si}), ionization threshold U_i equals to direct or stepwise ionization potential U_{di} or U_{si} , and the density of the colliding atoms (N_A) is either the gas density N or the excited state density taken equal to $N_m = 10^{11} \text{ cm}^{-3}$. The collision cross sections are the same as in our previous paper [8].

The kinetic equation (5) can be simplified by changing variables from U to the total energy ε since in new variables the mixed derivatives and projections of the electric field disappear. By introducing the total energy $\varepsilon = U - e\Phi(r, x)$, where $\Phi(r, x)$ is the two-dimensional spatial potential, and

substituting the anisotropic components into Eq. (5), we obtain the partial differential equation for the isotropic distribution,

$$\begin{aligned} & \frac{1}{r} \frac{\partial}{\partial r} A(\varepsilon, x, r) \frac{\partial f_0(\varepsilon, x, r)}{\partial r} + \frac{\partial}{\partial x} G(\varepsilon, x, r) \frac{\partial f_0(\varepsilon, x, r)}{\partial x} \\ & + \frac{\partial}{\partial \varepsilon} B(\varepsilon, x, r) f_0(\varepsilon, x, r) \\ & = C(\varepsilon, x, r) f_0(\varepsilon, x, r) - C(\varepsilon + U_{ex}, x, r) \\ & \times f_0(\varepsilon + U_{ex}, x, r) + D(\varepsilon, x, r) f_0(\varepsilon, x, r) - D_1 \\ & \times f_0(\varepsilon/\beta + U_i, x, r) - D_2 f_0(\varepsilon/(1-\beta) + U_i, x, r), \end{aligned} \quad (6)$$

with the coefficients defined as

$$A = \frac{U^2 N Q_\Sigma(U)}{U [N Q_\Sigma(U)]^2 + m \omega_{eB}^2 / 2},$$

$$G = \frac{U}{N Q_\Sigma(U)}, \quad B = 2 \frac{m}{M} U^2 N Q_{el}(U),$$

$$C = UNQ_{ex}(U), \quad D = \sum UN_A Q_i(U),$$

$$D_1 = \sum \left(\frac{U}{\beta} + U_i \right) \frac{N_A}{\beta} Q_i \left(\frac{U}{\beta} + U_i \right),$$

$$D_2 = \sum \left(\frac{U}{1-\beta} + U_i \right) \frac{N_A}{1-\beta} Q_i \left(\frac{U}{1-\beta} + U_i \right).$$

The total cross section $Q_\Sigma(U)$ is the sum of elastic, inelastic, and ionization cross sections, and the kinetic energy U is the function of the total energy and coordinates, $U = \varepsilon + e\Phi(x, r)$.

IV. CHARACTERISTIC SCALES

When employing a numerical solution of the Boltzmann kinetic equation for describing the electron component of magnetron discharge plasma, it is necessary to take into account the characteristic spatial scales of electron momentum and energy relaxation. These characteristic scales that determine the mechanisms of electron distribution formation are the free paths, energy relaxation lengths with respect to various collision processes, and plasma inhomogeneity scales.

The presence of the axial magnetic field, as it is seen from Eqs. (3) and (4), does not influence plasma in the axial direction but reduces electron drift velocity in radial direction by the factor of $1 + (\lambda_e/r_{ec})^2$. It is equivalent to reduction of the effective electron free path in the radial direction (λ_{eB}), which can be defined as $\lambda_{eB} = \lambda_e / [1 + (\lambda_e/r_{ec})^2]$, or to corresponding increase of an effective pressure.

The electron energy relaxation length may be understood as the distance at which electrons diffuse at the time τ_e of energy exchange in collisions,

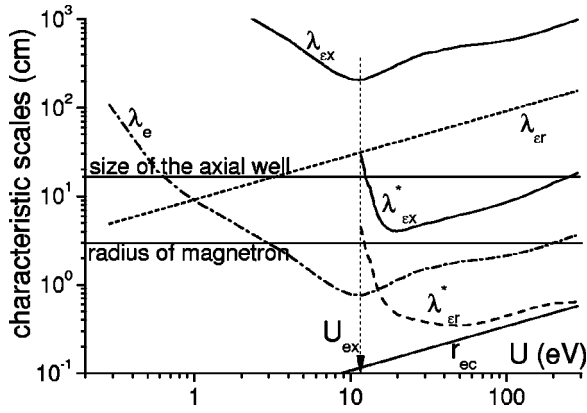


FIG. 2. Spatial scales of the electron motion and EDF formation in dependence on the electron kinetic energy. Ar, $p=3$ Pa, and $B=10$ mT.

$$\lambda_e \approx (D_{eB} \tau_e)^{1/2},$$

where $D_{eB} \sim v \lambda_{eB}/3$ is the electron diffusion coefficient in the direction perpendicular to magnetic field, and

$$\frac{1}{\tau_e} \approx v \left(\frac{m}{M} \frac{1}{\lambda_e} + \frac{1}{\lambda_e^*} \right),$$

with λ_e^* denoting electron free path with respect to inelastic collisions.

For the electrons whose energies are smaller than the excitation threshold, $U < U_{ex}$,

$$\lambda_e \approx \frac{(M/m)^{1/2} \lambda_e}{[1 + (\lambda_e/r_{ec})^2]^{1/2}} \approx \begin{cases} (M/m)^{1/2} \lambda_e \equiv \lambda_{ex}, & \lambda_e \ll r_{ec} \\ (M/m)^{1/2} r_{ec} \equiv \lambda_{er}, & \lambda_e \gg r_{ec}. \end{cases} \quad (7)$$

It is seen from Eq. (7) that the energy relaxation length is proportional to the free path for the unmagnetized electrons, and it is proportional to the electron cyclotron radius in strong magnetic fields ($\lambda_e \gg r_{ec}$, magnetized electrons).

For the electrons whose energies exceed the excitation potential, $U > U_{ex}$, under condition that $(M/m)\lambda_e \gg \lambda_e^*$, the energy relaxation length with respect to inelastic processes can be estimated as follows:

$$\lambda_e^* \approx \left(\frac{\lambda_e \lambda_e^*}{1 + (\lambda_e/r_{ec})^2} \right)^{1/2} \approx \begin{cases} \lambda_e (\lambda_e^*/\lambda_e)^{1/2} \equiv \lambda_{ex}^*, & \lambda_e \ll r_{ec} \\ r_{ec} (\lambda_e^*/\lambda_e)^{1/2} \equiv \lambda_{er}^*, & \lambda_e \gg r_{ec}, \end{cases} \quad (8)$$

with the similar dependence on magnetic field.

The characteristic scales are represented in Fig. 2 for Ar, at pressure $p=3$ Pa and magnetic field strength $B=10$ mT. For unmagnetized electrons moving in the axial direction, the energy relaxation length with respect to elastic collisions (λ_{ex}) much exceeds the discharge dimensions; the energy relaxation length with respect to inelastic collisions (λ_{ex}^*) is comparable with the size of the axial potential well. It means that slow electrons can travel many times across the axial potential well, without their total energy being noticeably

changed in elastic collisions. Large amount of fast electrons can also cross the axial well before they undergo excitation or ionization collision. For magnetized electrons moving in the radial direction, the energy relaxation length with respect to elastic collisions (λ_{er}) exceeds the radius of magnetron; the energy relaxation length with respect to inelastic collisions (λ_{er}^*) is short. As soon as the energy relaxation lengths are longer than the corresponding plasma inhomogeneity scales (discharge radius and size of the well), the electron distribution function at any point within the discharge gap is formed nonlocally both in the axial and radial directions by the whole two-dimensional profile of the potential rather than by the local electric field value.

Another important aspect of the electron distribution formation is the temporal scale of electron motion in the radial and longitudinal directions. In the axial direction the electrons are trapped by the potential well of the depth V_c . The time required for an electron to travel across this well of length L in diffusive regime can be estimated as $\tau_x \sim L^2/(v\lambda_e)$. In radial direction the electrons are heated by the radial field. To acquire a characteristic energy of the order of the electron temperature, kT_e they must travel the distance $\lambda_E = kT_e/eE_r$. The velocity of an energy acquisition for the transverse field configuration can be easily estimated as $v_E \sim eE_r/mv_E$, where $v_E = v/\lambda_{eB}$. Comparing the time of energy gain in radial field, $\tau_r = \lambda_E/v_E$, with the time of axial diffusive flights, we obtain

$$\frac{\tau_r}{\tau_x} \sim \left(\frac{kT_e}{eE_r L} \right)^2 \left(\frac{\lambda_e}{r_{ec}} \right)^2 \gg 1.$$

Thus, the axial displacement of an electron occurs faster than the energy gain or loss in radial field, and electron can travel many times across the axial potential well before it will gain noticeable energy (of the order of kT_e) from the radial field. This situation corresponds to explicit nonlocal formation of the EDF, when the total energy of an electron is approximately conserved during the axial motion, for $\tau_x \ll \tau_r$, $\lambda_{ex} \gg L$, and $\lambda_{ex}^* \gg L$. An effective treatment technique of the problems on the nonlocal formation of the electron distribution consists in averaging the corresponding kinetic equation over the spatial coordinate, along which the electrons are trapped and their total energy is conserved. The averaging procedure reduces the number of spatial dimensions, but the spatial information is retained implicitly. The methods of nonlocal kinetics and their applications to numerous gas discharge objects are summarized in Refs. [21,22].

V. SOLUTION OF THE KINETIC EQUATION

The nonlocal model will be applied to particular conditions of the CMD operation, that is Ar, $p=3$ Pa, $B=10$ mT, $i=150$ mA, discharge length $L=30$ cm, $R_C=0.9$ cm, and $R_A=3$ cm. The kinetic equation (6) will be solved in a model two-dimensional potential shown in Fig. 3 for half of the discharge length. The cathode and shields are at the potential of the cathode, which is taken here as equal to zero. The anode is an equipotential surface. The radial distribution of the potential at the center of the magnetron is

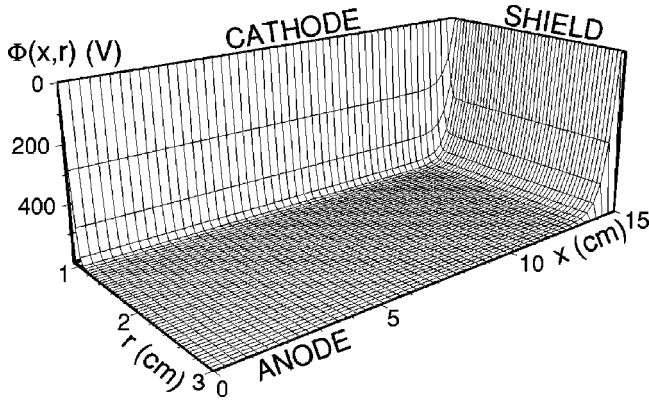


FIG. 3. Profile of the model potential for half of the cylindrical magnetron discharge. $R_C=0.9$ cm and $R_A=3$ cm. Shield is at the cathode potential, which is taken zero, anode is an equipotential surface. Factor n in Eq. (9) is taken equal to 40.

typical for potentials obtained self-consistently from the solutions of one-dimensional problems by nonlocal kinetic techniques [8]. In this study the radial distribution of the electric field at the CMD center is taken according to the two following conditions. First, the discharge voltage must correspond to experimentally measured $V_c=598$ V. Second, in frames of the one-dimensional (1D) axially uniform model [8] the radial course of the potential, $\varphi(r)$, must provide the radial profile of the electron density similar to the measured one. The trial radial electric field and the corresponding density profile at the discharge center are shown in Fig. 4. The measured density profile is shown in the figure by dots. The calculation results are normalized by the condition of current independence of axial position, $i=2\pi erj_0(r)L$, where $j_0(r)$ is the total current density.

The axial distribution of the potential is taken in the way that the boundary conditions at the cathode, shields, and anode are satisfied, and at the central part of the magnetron the potential is rather flat, which can be achieved by high value of the power n ,

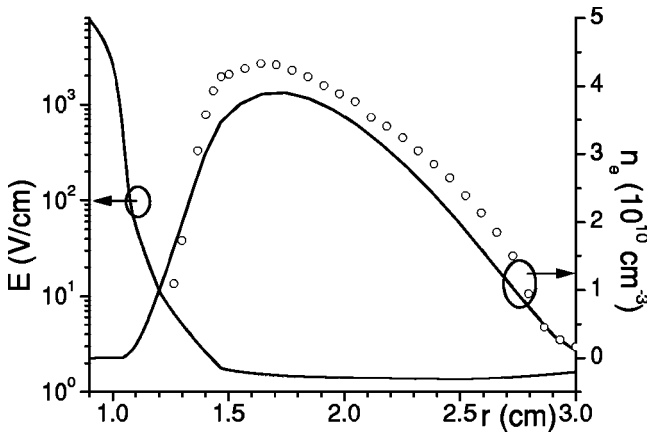


FIG. 4. Model electric field corresponding to potential at the discharge center (Fig. 3). Electron density is calculated in the model field in 1D approximation and measured density profile at the center.

$$\Phi(x,r) = \varphi(r) \left[1 - \left(\frac{x}{L/2} \right)^n \right]. \quad (9)$$

Thus, according to experiments [19], at the central region of magnetron the radial profiles of the potential are almost identical. At the discharge periphery there is the potential well which traps the electron motion in axial direction.

As soon as the energy relaxation length in the axial direction considerably exceeds the length of the magnetron, the EDF is formed by whole axial potential. Electrons travel across the axial well many times before they acquire energy in the radial field. The kinetic equation (6) can be averaged over axial coordinate to yield the following representation:

$$\begin{aligned} \frac{1}{r} \frac{\partial}{\partial r} r A(\varepsilon, r) \frac{\partial f_0(\varepsilon, r)}{\partial r} + \frac{\partial}{\partial \varepsilon} B(\varepsilon, r) f_0 &= \overline{C(\varepsilon, r)} f_0 \\ &- \overline{C(\varepsilon + U_{ex})} f_0(\varepsilon + U_{ex}, r) + \overline{D(\varepsilon, r)} f_0(\varepsilon, r) \\ &- \overline{D_1} f_0(\varepsilon/\beta + U_i, r) - \overline{D_2} f_0(\varepsilon/(1-\beta) + U_i, r). \end{aligned} \quad (10)$$

The average of the coefficients is carried out according to the rule

$$\overline{H(\varepsilon, r)} = \frac{2}{L} \int_0^{x_0(\varepsilon, r)} H(\varepsilon, x, r) dx,$$

where the surface $x_0(\varepsilon, r)$ limits the region reachable for electrons, i.e., the kinetic energy turns to zero at this surface (turning points). The second term of Eq. (6) vanishes in the averaging procedure due to the central symmetry of the discharge and the boundary condition at the potential well $x_0(\varepsilon, r)$:

$$\frac{U}{NQ_\Sigma} \frac{\partial f_0}{\partial x} \Big|_{x_0(\varepsilon, r)} = 0.$$

An explicit axial dependence of the EDF vanishes, and the remaining variables are the total energy and radius.

The methods for solving the partial differential equations of the form of Eq. (10) were described in Ref. [8]. The equation can be discretized on a grid that is equidistant in total energies and nonequidistant in radius. Large gradients of electric field and the necessity of an accurate treatment of ionization collisions require one to use the grids with a small step in energy. The accuracy of the obtained results was checked by a requirement of fulfillment of axially averaged particle and energy balances.

The solution of the averaged kinetic equation yields the EDF at the center as a function of the total energy and radial coordinate. The electron distributions at the axial points that are distanced by x_k from the center can be obtained by the rearrangement of the variables of the axial EDF according to the potential $\Phi(x_k, r)$. This procedure is analogous to calculations of the nonlocal distribution functions in the positive column of a discharge [23].

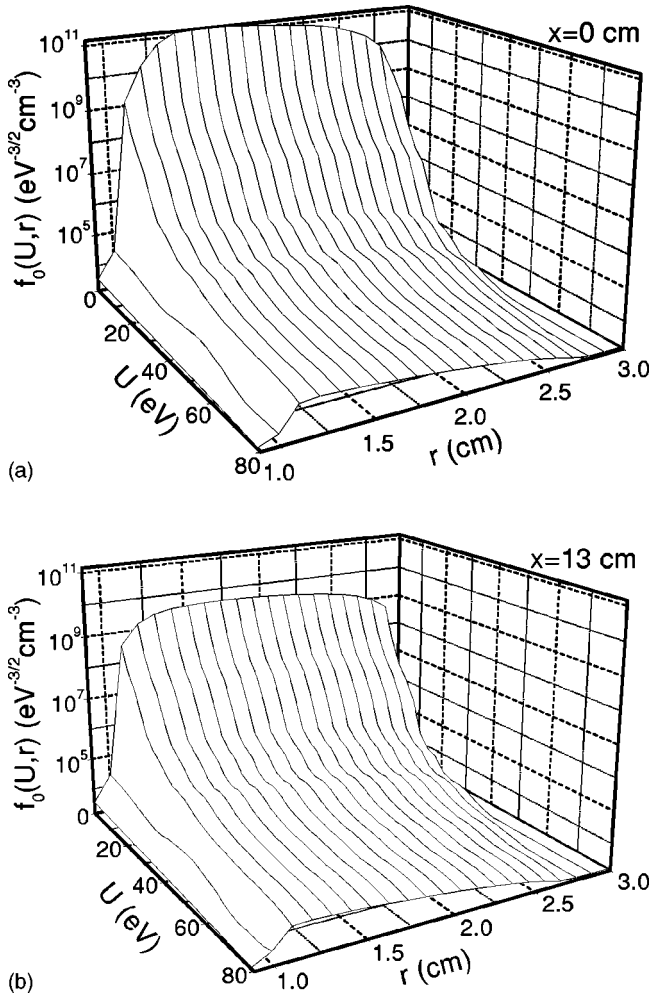


FIG. 5. EDFs as the functions of the kinetic energy and radial position at the discharge center (a) and 13 cm aside (b).

VI. RESULTS AND DISCUSSION

The resultant EDFs for the central point and at 13 cm from the center are shown in Fig. 5. The radial fall of the potential in quasineutral plasma region is small, almost whole discharge voltage is applied to the cathode region. For this reason, the axial transformation of the electron distribution is connected mostly with the EDF decrease in the absolute value. A shift of a radial position of maximum in slow electrons that are responsible for electron particle and current density, and of maximum in fast electrons that contribute to ionization and excitation rates, becomes more apparent at larger values of x .

Using the EDFs at different axial positions, the radial profiles, for instance, of the electron density (n_e) and ionization rate (I) can be calculated as the functions of the axial position and radius according to

$$n_e(x, r) = \int_{-e\Phi(x, r)}^{\infty} f_0(\varepsilon, r) [\varepsilon + e\Phi(x, r)]^{1/2} d\varepsilon, \quad (11)$$

$$I(x, r) = \left(\frac{2}{m}\right)^{1/2} \sum \int_{U_i - e\Phi(x, r)}^{\infty} N_A Q_i (\varepsilon + e\Phi(x, r)) \times f_0(\varepsilon, r) [\varepsilon + e\Phi(x, r)]^{1/2} d\varepsilon. \quad (12)$$

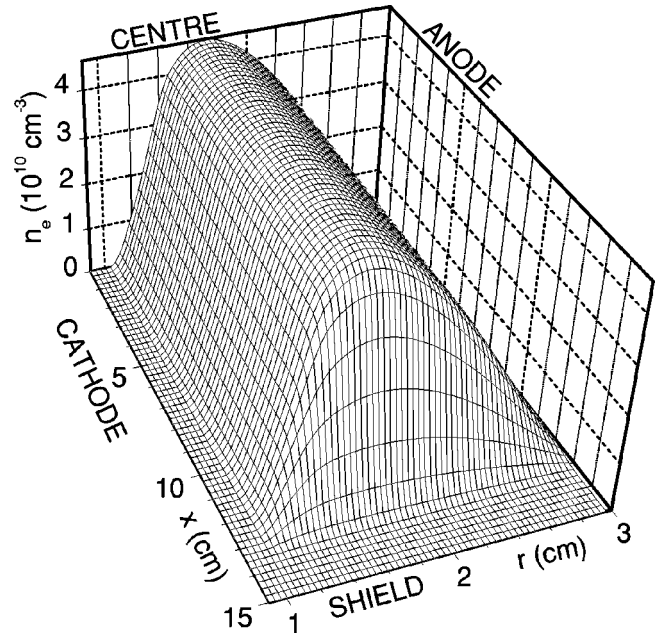


FIG. 6. Electron density as a function of the axial and radial coordinates.

The 3D graphs of the electron density and ionization rate are shown in Figs. 6 and 7. The radial profiles at the discharge center ($x=0$) are similar to those obtained in our previous works as well as to those computed by the PIC [5]. The particle density attains its maximum in the region of the field's minimum and then decreases towards the anode. The rate of ionization is maximal approximately at the boundary of the cathode-fall and negative glow regions. At the central part of the discharge, the radial distributions of the plasma properties are almost identical for different axial positions. In

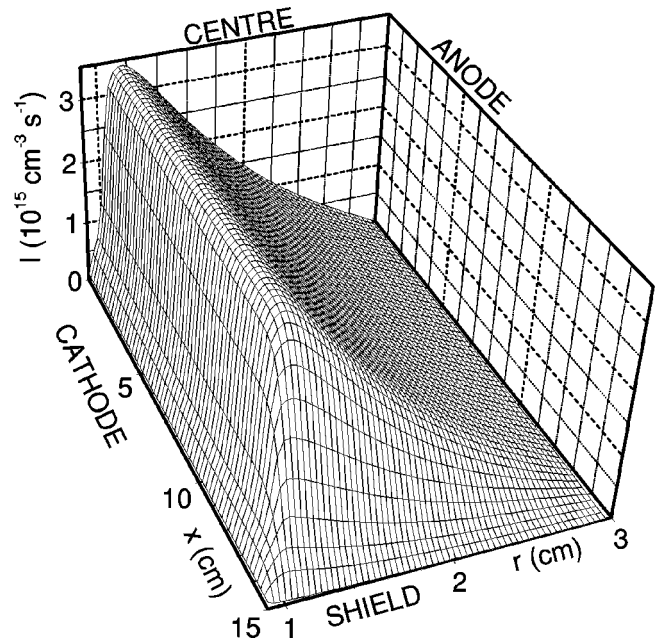


FIG. 7. Ionization rate as a function of the axial and radial coordinates.

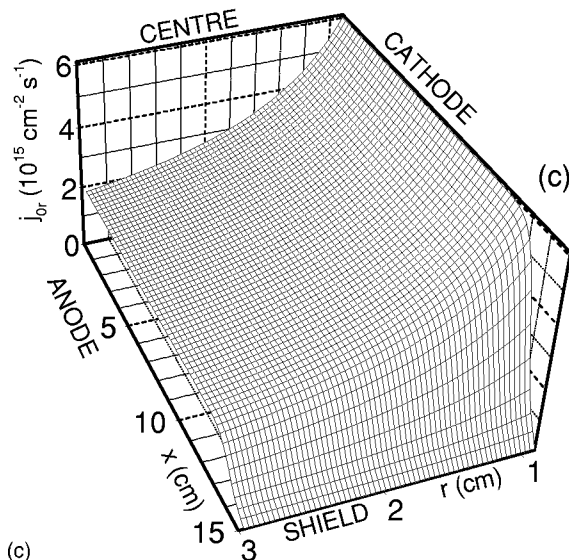
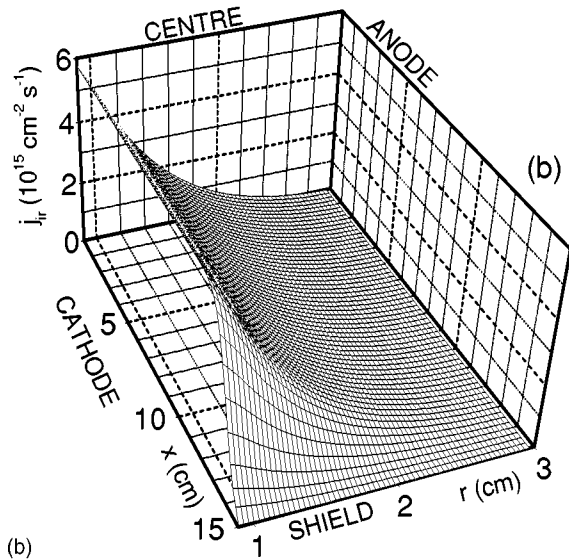
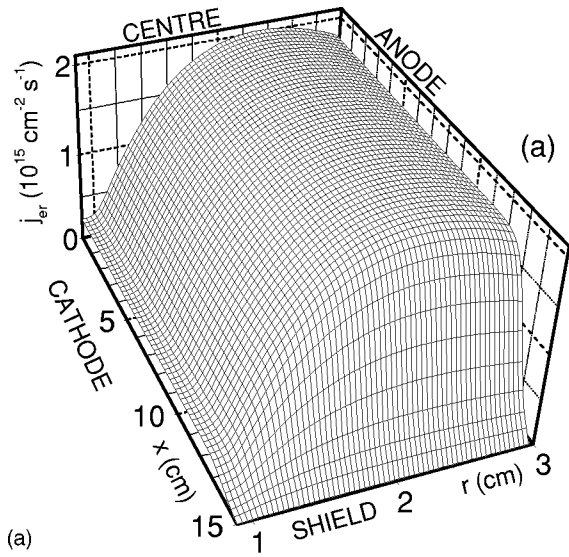


FIG. 8. Electron (a), ion (b), and total (c) radial current densities as functions of the axial and radial coordinates.

the periphery region there is a decrease towards the shields. Electrons are reflected from the walls of the axial potential well. The decrease of the ionization rate starts at smaller axial coordinates than the decrease of the density. This is caused by depletion of the nonlocal distribution function in fast electrons.

The two-dimensional profiles of the radial current densities can be computed from the ionization rate distributions. Due to the boundary condition used in the average procedure, there is no axial component of the electron currents in our model. The axial component of the ion current density can be neglected compared to the radial component, since the discharge is axially homogeneous in the central part, and the current to the shields (as the experiments [19] show) is few hundredths of the current to the cathode. The ion radial current density that satisfies the condition $j_i(x, r=R_A)=0$, under the approximation of smallness of the axial ion current density, can be written as

$$j_{ir}(x, r) = \frac{1}{r} \int_r^{R_A} I(x, r) r dr. \quad (13)$$

At the cathode surface the electron and the ion current densities are related by the condition $j_e = \gamma j_i$, where γ is the electron secondary emission coefficient. The electron current density can be calculated as

$$j_{er}(x, r) = \frac{R_C}{r} \gamma j_{ir}(x, R_C) + \frac{1}{r} \int_{R_C}^r I(x, r) r dr. \quad (14)$$

The charged particle current densities are combined into the total current density j_{0r} ,

$$j_{0r}(x, r) = j_{er}(x, r) + j_{ir}(x, r),$$

which is connected with the discharge current by

$$i = 2\pi e \cdot 2 \int_0^{L/2} j_{0r}(x, r) r dx. \quad (15)$$

The 3D graphs of the electron, ion, and total radial current densities are shown in Figs. 8(a)–8(c). Note that the product $j_{0r}(x, r)r$ is independent of r , which is stipulated by the discharge geometry. The values of current linear density

$$i_x = 2\pi e j_{0r}(x, r) r \quad (16)$$

give the current at the axial point x .

The comparison of the calculated and measured dependences is given in Fig. 9. The solid curve in Fig. 9(a) is the calculated radial profile of the electron density at the center of the CMD, and it is compared with the measured values (solid dots). Open dots are the measured electron density profile at 12 cm aside from the center, where the third probe is positioned. The dashed curves are the calculations at 12 cm (upper curve) and 12.2 cm (lower curve). In Fig. 9(b) we compare the calculated and measured axial profiles of the currents falling on the cathode surface. Dots are the measurements [19] of the current on the segments and the line is a computation according to Eq. (16). Both measured and cal-

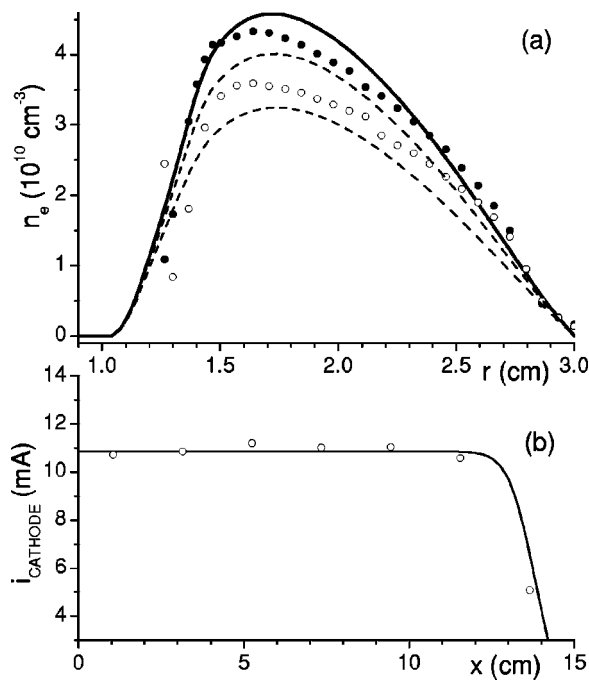


FIG. 9. Calculated (lines) and measured (dots) electron densities at the CMD center (solid) and at 12 cm aside from the center (open). Dashed lines are calculational results at $x=12$ cm (upper line) and $x=12.2$ cm (lower line)(a). Calculated (line) and measured (dots) axial distributions of the current on cathode (b).

culated values are multiplied by 2 being drawn for half of the discharge. It is seen that in the frames of the half-empirical model, where input parameters are the discharge voltage, the approximate radial course of the field, and the power n of the axial dependence of potential, the obtained axial variations of the particle density and current to cathode agree well with the experiment.

In principle, the various kinds of instabilities can develop in the magnetized plasma. As a rule, the plasma instabilities appear in sufficiently strong magnetic fields when the field strength exceeds some critical value. The presence of stochastic instabilities has been detected in our CMD when the magnetic field increased above the value of approximately 20 mT [24]. These oscillations had the continuous frequency spectrum, and manifest as the unwanted noise added to the Langmuir probe floating potential when measuring with the floating probe, and as the increased noise of the measured current when measuring the V - A probe characteristic. Under our experimental conditions of low magnetic fields, the oscillations can be believed to play no significant role. Nevertheless, extensive experimental and theoretical studies are required concerning the possibility and the role of instabilities.

VII. CONCLUSION

The cylindrical magnetron discharge with the large ratio of length to radius has been designed to create axially uniform regions where all parameters are only radially varying. The measurements of the axial dependence of the electron density and currents on cathode showed that there are significant disturbances of plasma produced by the shields limiting the discharge in the axial direction and biased at the cathode potential. The presence of the shields creates axial potential well that traps electrons in the central region of CMD. Under low pressures and small magnetic fields used in experiments, the electron energy relaxation lengths considerably exceed the magnetron radius (for magnetized electrons) and the length of the CMD (for unmagnetized electrons), yielding strongly nonlocal distribution functions. The spatially inhomogeneous Boltzmann kinetic equation has been employed for the numerical analysis of the electron motion. As the electron travels many times across the axial potential well before its energy is changed noticeably due to acceleration in radial electric field, the average of the kinetic equation over axial coordinate appears to be an effective solving procedure. The averaged kinetic equation can be solved numerically, being formally alike the nonaveraged equation written under assumption of the axial homogeneity of the discharge. The resultant electron distribution function depends on the total energy and radial coordinate, and it can be recalculated in terms of the kinetic energy and radius for every axial coordinate by corresponding rearrangement of the variables. The electron density and ionization rate calculated from this EDF decrease in approaching towards the shields. The current linear density, i.e., the current on cathode surface also demonstrates falling axial dependence. The comparison of the calculated axial dependences of electron density and current on cathode showed good agreement with the experimental results.

ACKNOWLEDGMENTS

The work was financially supported by the DFG SFB 198 Greifswald “Kinetik partiell ionisierter Plasmen,” Grant No. PD02-1.2-17 by the Russian Ministry of Education, DAAD trilateral project of Universities of Greifswald, St. Petersburg and Paris-Sud, the Grant Agency of the Czech Republic, Grant Nos. GACR-202/00/1689, GACR-202/03/0827, GACR-202/01/D095, by the Grant Agency of Charles University, Grant No. 171/2000/B FYZ/MFF, and by the Ministry of Education, Youth and Sports, Research Grant No. MSM 113200002.

[1] A.E. Wendt, M.A. Lieberman, and H. Meuth, *J. Vac. Sci. Technol. A* **6**, 1827 (1988).
 [2] L. Pekker, *Plasma Sources Sci. Technol.* **4**, 31 (1995).
 [3] J.W. Bradley and G. Lister, *Plasma Sources Sci. Technol.* **6**,

524 (1997).

[4] S. Kondo and K. Nanbu, *J. Phys. D* **32**, 1142 (1999).
 [5] T.A. van der Straaten, N.F. Cramer, I.S. Falconer, and B.W. James, *J. Phys. D* **31**, 177 (1998).

- [6] D. Gracin, R. Denkelmann, S. Maurmann, and Z. Andreic, *Contrib. Plasma Phys.* **40**, 120 (2000).
- [7] J.F. Behnke, C. Csambal, J. Ruzs, P. Kudrna, and M. Tichý, *Czech. J. Phys.* **50/S3**, 427 (2000).
- [8] I.A. Porokhova, Yu.B. Golubovskii, J. Bretagne, M. Tichý, and J.F. Behnke, *Phys. Rev. E* **63**, 056408 (2001).
- [9] C.H. Shon, J.K. Lee, H.J. Lee, Y. Yang, and T.H. Chung, *IEEE Trans. Plasma Sci.* **26**, 1635 (1998).
- [10] N.F. Cramer, *J. Phys. D* **30**, 2573 (1997).
- [11] F. Debal, J. Bretagne, J.P. Dauchot, M. Hecq, and M. Wautelet, *Plasma Sources Sci. Technol.* **10**, 30 (2001).
- [12] J.W. Bradley, H. Bäcker, Y. Aranda-Gonzalvo, P.J. Kelly, and R.D. Arnell, *Plasma Sources Sci. Technol.* **11**, 165 (2002).
- [13] J.F. Behnke, E. Passoth, C. Csambal, M. Tichý, P. Kudrna, D. Trunec, and A. Brablec, *Czech. J. Phys.* **49**, 483 (1999).
- [14] E. Passoth, P. Kudrna, C. Csambal, J.F. Behnke, M. Tichý, and V. Helbig, *J. Phys. D* **30**, 1763 (1997).
- [15] E. Passoth, J.F. Behnke, C. Csambal, M. Tichý, P. Kudrna, Yu.B. Golubovskii, and I.A. Porokhova, *J. Phys. D* **32**, 2655 (1999).
- [16] J.F. Behnke, J. Ruzs, P. Kudrna, and M. Tichý, in *Proceedings of the ICPP-2000, Quebec, Canada*, edited by R. Decoste *et al.* (Hydro-Quebec and INRS, Quebec City, 2001), Vol. 2, p. 944.
- [17] I.A. Porokhova, Yu.B. Golubovskii, C. Csambal, V. Helbig, C. Wilke, and J.F. Behnke, *Phys. Rev. E* **65**, 046401 (2002).
- [18] P. Kudrna, M. Holik, and M. Tichy, *Czech. J. Phys.* **52**, Suppl. A, D666 (2002).
- [19] P. Kudrna, M. Tichy, J.F. Behnke, C. Csambal, and J. Ruzs, in *Proceedings of the 15th ISPC, Orleans, France*, edited by A. Bouchole *et al.* (Gremi Laboratory, Orleans, France, 2001), Vol. 4, p. 2119.
- [20] G. Petrov and R. Winkler, *J. Phys. D* **30**, 53 (1997).
- [21] L.D. Tsendin, *Plasma Sources Sci. Technol.* **4**, 200 (1995).
- [22] V.I. Kolobov and V.A. Godyak, *IEEE Trans. Plasma Sci.* **23**, 503 (1995).
- [23] Yu.B. Golubovskii, I.A. Porokhova, J. Behnke, and J.F. Behnke, *J. Phys. D* **32**, 456 (1999).
- [24] P. Kudrna and E. Passoth, *Contrib. Plasma Phys.* **37**, 417 (1997).